Influence of temperature changes and vertically transported trace species on the structure of MLT region during major SSW events

Akash Kumar [a], M.V. Sunil Krishna [a,*], Alok Kumar Ranjan [a], Stefan Bender [b], Miriam Sinnhuber [c], Sumanta Sarkhel [a]

[a] Department of Physics, Indian Institute of Technology Roorkee, Roorkee, 247667, Uttarakhand, India
[b] Instituto de Astrofisica de Andalucia (CSIC) Glorieta de la Astronomia s/n, 18008, Granada, Spain
[c] Institute of Meteorology and Climate Research, Karlsruhe Institute of Technology, Karlsruhe, Germany

Keywords:
Stratospheric warming
Mesospheric cooling
Nitric oxide
Secondary ozone
Circulation change

A B S T R A C T

Sudden stratospheric warming (SSW) events are large-scale dynamic phenomena which can significantly affect the circulation, temperature, and composition of different atmospheric layers. The circulation changes during these events induce variations in the atmospheric neutral and ion densities and cause the vertical transport of various trace species. The severity of effects induced by major SSW events in the mesosphere and lower thermosphere (MLT) region has received less attention than that in the lower atmosphere. The major influence of temperature and vertically transported trace species on the energetics, thermal and compositional structure of the MLT region has been investigated during two major SSW events with elevated stratopause. Variations in the nitric oxide volume emission rates (NO-VER), a measure of infrared radiative cooling by NO, are reported for the first time in the context of the dynamical changes during SSW events. This study investigates the role of temperature and NO variability on the energetics of the MLT region, particularly during the formation of elevated stratopause. The effects of supplemented NO density on the secondary ozone layer has also been investigated during these events, the anti-correlation between secondary ozone and NO does not conclude on the role of NO in the secondary ozone peak density variations. Notwithstanding the similarity in terms of defining characteristics, both SSW events impact the secondary ozone layer differently. In contrast to earlier studies, it is suggested that along with temperature, the availability of atomic oxygen is the major factor for the observed variation in secondary ozone during the SSW events.

1. Introduction

Nitric oxide (NO), a highly variable trace species in Earth's atmosphere, plays a crucial role in the energy budget of the mesosphere and lower thermosphere (MLT). Barth (1992), Mlynczak et al. (2003), and Sharma et al. (1996) have discussed the critical role of NO in the thermal and compositional structure of the MLT region due to its lowest ionization potential. The infrared-active (IR-active) vibrational modes of NO help in regulating temperatures, mainly in the MLT region, by absorbing excess energy and re-radiating in the infrared spectrum. The 5.3 μm emission from NO acts as a natural thermostat, balancing the temperature variations by providing radiative cooling primarily during geomagnetic storm conditions (Mlynczak et al., 2003). Therefore, the temperature sensitivity of NO emissions (Kockarts, 1980) makes it a good cooling agent and an indicator to observe the effects of external forcing on the MLT region. It is evident from the earlier studies that, among other IR-active molecules, emissions from NO play a crucial role in the cooling of the MLT region during extreme space weather and geomagnetic events (Ogawa, 1976; Mlynczak et al., 2010; Ranjan et al., 2023).

Due to the negligible photodissociation during polar winter nights, the increased photochemical lifetime of NO helps it be controlled by atmospheric dynamics as well. The variation in the NO and its emission in the mesosphere may affect the mesospheric cooling, and the descent of NO can contribute to the change in the stratospheric ozone (Solomon et al., 1982). Randall et al. (2009) indicated that during the year 2009, under low geomagnetic activity conditions, about 50-time enhancement in NO_x was observed in the stratosphere because of vertical transport, which could lead to the ozone (O_3) depletion. In contrast to this, Salmi et al. (2011) suggested that O_3 depletion in the stratosphere was not due to high NO_x descending amounts but rather was due to increased solar radiation and activation of halogen and hydroxyl (HO_x) compounds in the late winters. Therefore, the vertical

* Corresponding author.
E-mail address: mv.sunilkrishna@ph.iitr.ac.in (M.V. Sunil Krishna).

transport of trace species such as NO, and their effects on other trace species such as O_3 are not completely understood.

Solar radiation causes photolysis of molecular oxygen (O_2) and produces atomic oxygen (O), which participates in the O_3 formation by a three-body reaction throughout the middle atmosphere (De Grandpré et al., 2000). Variations in the hydrogen (H) and oxygen in the photochemical reactions influence the O_3 concentration in the middle atmosphere. The maximum abundance of O_3 near the mesopause is, therefore, caused by a balance of the photolysis of oxygen molecules producing a large amount of O_3 competing against the continuing loss of hydrogen (Smith and Marsh, 2005). The O_3 peak around 90–100 km is known as the "secondary ozone layer" and is maintained by photochemical equilibrium, which is much more abundant near the mesopause at night due to reduced photolytic destruction (Smith and Marsh, 2005). Several observational studies have primarily focused on the mesospheric O_3 variation due to dynamic changes during extreme dynamic events; however, the effects of other trace species' variation during these events have some uncertainty (Smith et al., 2009, 2014; Tweedy et al., 2013). Based on the discussion above, we conclude for now that the middle atmospheric dynamics have a prominent influence on mesospheric NO and O_3 abundance. Therefore, it is important to study the NO and O_3 variability with temperature and circulation-induced composition change into the middle atmosphere during extraordinary dynamic events for a better understanding of the mesospheric thermal structure and chemistry of trace species.

Sudden Stratospheric Warming (SSW) events are common among these dramatic dynamic events in which stratospheric temperature increases by several tens of Kelvins with the decline or sometimes reversal of wintertime stratospheric circulation in the polar region (Baldwin et al., 2021; Chandran et al., 2014; Scherhag, 1960; Schoeberl, 1978). Vertically propagating quasi-stationary planetary scale waves (Rossby waves) interact with the stratospheric mean flow, which slows down or sometimes reverses the wintertime eastward winds and opposes wave-induced motion in the stratosphere, resulting in residual downwelling and therefore a dramatic warming in the polar stratosphere. This sequence of events defines the occurrence of an SSW event (Charney and Drazin, 1990; Matsuno, 1971). Recent studies tried to broaden and update the definition of SSW since their identification is sensitive to the latitudes, wind speed threshold, pressure level, and preconditioning of the stratosphere (Butler et al., 2015; Butler and Gerber, 2018; Charlton and Polvani, 2007; de la Cámara et al., 2017; Limpasuvan et al., 2004).

The impact of SSW events is not only experienced in the polar stratosphere; they reaching up to troposphere (Kodera et al., 2016; Nath et al., 2016; Rao et al., 2020). Various effects on the structure, dynamics, and composition of the mesosphere, lower thermosphere, and ionosphere has been reported earlier (Bailey et al., 2014; Damiani et al., 2010; Goncharenko et al., 2010; Gong et al., 2016, 2021; Ma et al., 2022; Koushik et al., 2018; Randall et al., 2006; Yamazaki et al., 2015). A positive correlation between air temperature and underground muon flux was also reported during these events (Varotsos et al., 2010). There have been several studies that have tried to explore this vertical coupling, and they attribute the reason for this connection mainly to the zonal mean circulation change due to variation in gravity wave filtering (Chandran et al., 2014; Holton, 1983; Limpasuvan et al., 2016; Nayak and Yiğit, 2019; Yiğit et al., 2016). The reversal of mesospheric circulation can happen readily due to additional wave forcing from the lower atmosphere and their interaction with the weak background flow, which may result in an independent meridional circulation (Iida et al., 2014; Laskar et al., 2019). This circulation rapidly propagates downward into the upper stratosphere and lower mesosphere (USLM) and distorts the polar vortex and stratospheric mean structure. The reversed stratospheric circulation allows the propagation of the westward gravity waves into the mesosphere. The net planetary wave forcing dominating westward gravity waves drag results in the polar downwelling that produces adiabatic warming and reforms the stratopause at mesospheric altitudes, known as elevated stratopause (ES) (Chandran et al., 2014; Limpasuvan et al., 2012, 2016).

The vortex breakdown and downwelling from the mesosphere to the stratosphere affect the composition of these regions via increased vertical transport of trace species (Bailey et al., 2014; Randall et al., 2009; Wang et al., 2019), and air mixing between polar and extra-polar regions (Manney et al., 2009). The enhanced polar mesospheric temperature and the vertical transport-led descent of trace species into an unusually strong re-established USLM vortex can cause the increased destruction of polar stratospheric O_3 (Solomon et al., 1982). The variations in the hydroxyl (OH) layer were also found to be associated with the mesospheric temperature and odd oxygen (O_x) variations during the winters with an SSW (Damiani et al., 2010), but variations in the secondary O_3 layer in the mesosphere and lower thermosphere (MLT) are not completely understood in relation to temperature or trace species concentration changes (Smith et al., 2009). Earlier studies mainly focused on the transport of trace species from the thermosphere into the mesosphere during SSW events, but the impact of these transported species on the composition and thermal structure still remains unclear. Hence, it is very important to address the role of circulation changes, temperature changes, and transport on the abundance of NO, resulting in 5.3 μm emission and on O_3 during these extraordinary dynamic events. Tweedy et al. (2013) reported the qualitative study of variability of the secondary O_3 layer using the "Specified Dynamics" version of the Whole Atmosphere Community Climate Model (SD-WACCM) for several major SSW events with elevated stratopause. In their composite analysis, the effect of some major SSW events accompanied by minor SSW events, and their severity have not been addressed. The reason for the underestimation of the secondary O_3 maximum values in their SD-WACCM simulation also remains unclear. Therefore, a quantitative analysis of the variability of trace species during every individual SSW event is required to understand the complexity of dynamics, which play a differential role in each SSW event. To clarify the mutual impact of the trace species on one another since every SSW event influences the atmosphere differently, which is also evident in our results. Since the timing of SSW events affects vertical transport as well (Holt et al., 2013), we have selected two SSW events during 2006 and 2009 which occurred at around the same time.

The present study focuses on understanding the variations in the mesospheric and lower thermospheric NO abundance, its 5.3 μm emission, and O_3 abundance in the MLT region due to temperature and circulation change induced transport during major SSW events accompanied by elevated stratopause (SSW-ES) occurred in mid-winter. As mentioned earlier, the vertically transported NO can influence the radiative cooling and middle atmospheric O_3. The results pertaining to the impact of vertically transported NO and O on the NO volume emission rates (VER, erg.cm^{-3}.s^{-1}) and mesospheric O_3 over the polar region during these major SSW-ES are presented. The finding suggests the differential response of the MLT region towards two major SSW-ES events.

2. Data and methodology

2.1. Sounding of the atmosphere using broadband emission radiometry (SABER)

SABER onboard NASA's TIMED (Thermosphere, Ionosphere, Mesosphere, Energetics, and Dynamics) satellite, launched in December 2001, provides the measurement of infrared (IR) and near-IR emissions from several atmospheric constituents (Mlynczak, 1997). The TIMED satellite is in a nearly circular orbit with an inclination of 74° at about 625 km altitude. SABER is a ten-channel broadband IR (1.27 to 16.9 μm) radiometer that provides near-global radiance data of the earth's limb on a daily basis. SABER obtains profiles from 52°S to 83°N for about 60 days during its north-viewing mode and switches its viewing mode to the south (measuring from 52°N to 83°S) after

60 days and repeats this sequence for subsequent time periods. SABER has an altitude coverage of 10 km to 180 km with a 0.4 km limb vertical sampling interval. The details about the SABER instrument can be found in Russell et al. (1999). The SABER data is widely used in earlier studies and validated (Bharti et al., 2018; Mlynczak et al., 2003; Ranjan et al., 2023; Shepherd et al., 2014; Smith et al., 2009). Additionally, Varotsos and Efstathiou (2018) also verified the SABER dataset by examining long-term variations in the power emitted by NO and carbon dioxide CO_2 from the thermosphere, thus enhancing the reliability of the SABER dataset.

The temperature is obtained from the 15 μm emission of CO_2, which is in local thermodynamic equilibrium (LTE) in the stratosphere and lower mesosphere. The temperature and O_3 data from SABER are available from nearly 15 km to 110 km altitude range, whereas O and H data are available from about 40 km to 110 km altitude range. In this study, we have employed temperature, O_3, O, and H from the SABER data version v2.0 for 2006 (displaced vortex type) and 2009 (split vortex type) major SSW events with ES, in the north viewing mode of SABER over the polar region. For a given latitude and altitude range, both the ascending and descending orbital profiles with daytime and nighttime data are included in the daily averaged time series of various parameters.

2.2. Whole Atmosphere Community Climate model with thermosphere–ionosphere eXtention (WACCM-X)

WACCM is a comprehensive numerical model that is developed using the National Center for Atmospheric Research's (NCAR) Community Earth System Model (CESM) (Marsh et al., 2013). WACCM-X is the thermospheric and ionospheric extension of the WACCM, and its output data has been used for winds in the present study. The upward extension is from the surface of the earth up to between 500 and 700 km altitude, depending on the solar activity, which is the top boundary of this model. Above 0.96 hPa, vertical resolution has been increased to one-quarter scale height with the top pressure (p) of 4.1×10^{-10} hPa.

WACCM-X includes neutral wind dynamo, ionospheric transport, and calculation of ion/electron energetics and temperatures. Parameterized non-orographic gravity waves forcing revision and improvements related to SSW frequency (Garcia et al., 2017) are also included. The tropospheric and stratospheric dynamics can be constrained in WACCM-X by the specified-dynamics (SD) version of the model, which was broadly used to study SSW (Chandran et al., 2014; Smith et al., 2011). The self-consistently resolving lower atmospheric processes in the WACCM-X 2.0, enables a more realistic simulation of upper atmospheric variability due to lower atmospheric forcing. The details of the WACCM-X model are given by Liu et al. (2018).

The winds in the stratosphere and mesosphere are presented using daily mean zonal, meridional, and vertical wind (converted from Pa/s to m/s) data from WACCM-X daily output that were released as part of NCAR-CESM version 2. The daily output files contain the specified dynamics (SD) WACCM-X version v2.1 simulation with the nudging of Modern-Era Retrospective analysis for Research and Applications, Version 2 (MERRA-2) data from the surface up to 50 km. The details about the SD-WACCM-X daily output file and the data utilized for this study can be found at: https://www.earthsystemgrid.org/dataset/ucar.cgd.ccsm4.SD-WACCM-X_v2.1.html. The meridional and vertical residual winds, v and w, have been calculated for the selected SSW events by taking the difference between the quiet-time mean values before the SSW-ES onset and the actual values of the corresponding wind components. The quite-time mean/pre-SSW values are the averaged values of the utilized quantities from the day of available SABER observation in north viewing mode to the day before SSW-onset (approx. one week).

2.3. Scanning Imaging Absorption spectroMeter for Atmospheric CartograpHY (SCIAMACHY)

The NO density variation in the mesosphere and lower thermosphere during the northern hemispheric polar winters of 2006 and 2009 has been analyzed using nitric oxide number density data from SCIAMACHY. SCIAMACHY, onboard ESA's ENVISAT satellite launched on March 1, 2002, is an imaging spectrometer with a moderate resolution that measures reflected and transmitted sunlight by the Earth's atmosphere in a wide wavelength range (240–2380 nm) (Bovensmann et al., 1999; Burrows et al., 1995). SCIAMACHY observes scattered and reflected radiance in limb and nadir geometry and transmitted radiance in solar and lunar occultation geometry. The main objective of the SCIAMACHY mission was to study the physics and chemistry of the Earth's atmosphere to improve our understanding of global atmospheric composition changes. SCIAMACHY has eight high-resolution channels that provide measurements of a large number of atmospheric constituents. SCIAMACHY retrieves the NO density in the upper mesosphere by observing the gamma bands of NO using UV channel 1 (230–314 nm) (Bender et al., 2017b). More details of the SCIAMACHY instrument can be found in Bovensmann et al. (1999) and the references therein. The SCIAMACHY data is available at the data-set record developed by Bender et al. (2017a).

NO-VER has also been calculated as per the scheme detailed in Khomich et al. (2008) using NO density obtained from SCIAMACHY, while temperature and O density are used from the SABER dataset. The other important species densities are obtained using the NRLMSISE-00 model (Picone et al., 2002). The oxygen molecule ion (O_2^+) concentration is obtained from the IRI model. The facility of online-run for NRLMSISE-00 and IRI-2016 models to get data is also available at https://ccmc.gsfc.nasa.gov/. Since the excitation processes of NO emission are thermal in nature (Ogawa, 1976), the fluorescence caused by the solar radiation and the earthshine has been neglected in the NO-VER calculations for the selected polar night periods.

This study examines two robust major SSW events with ES that occurred at the same time (~23 January) in 2006 and 2009, employing simultaneous observational data from SCIAMACHY (available between 2002 and 2012) and SABER in north viewing mode (~10 January - ~10 March) during the norther polar winter, and WACCM-X modeled outputs. The entire duration of an SSW event is divided into three phases: SSW onset when circulation starts to change in the mesosphere and zonal wind reverses at 1 hPa level; the main phase when temperature and circulation remain reversed in the stratosphere and mesosphere; and finally the recovery phase when characteristic wintertime circulation is re-established in the USLM.

3. Results and discussion

3.1. Major SSW events, their characteristics, and effects on temperature and circulation

In order to understand the effect of major stratospheric warming events on radiative cooling by NO over the northern polar region, two major SSW events with ES (SSW-ES) occurred during the mid-winter of the years 2005–2006 and 2008–2009 are considered in the present study. These two events are referred to as the 2006 SSW and 2009 SSW events. The 2006 event was a major SSW-ES event preceded by a minor SSW event that occurred several days prior to the major SSW-ES event. The atmosphere has been significantly impacted by these SSW events. The characteristic features of these warming events are established using the SABER measurement and WACCM-X model output data. The daily averaged zonal mean temperature between 70° and 80° N, obtained from SABER measurements, and the zonal mean winds daily averaged at the SSW defining latitude (60° N), derived from the WACCM-X model output data during these winters are shown in Fig. 1.

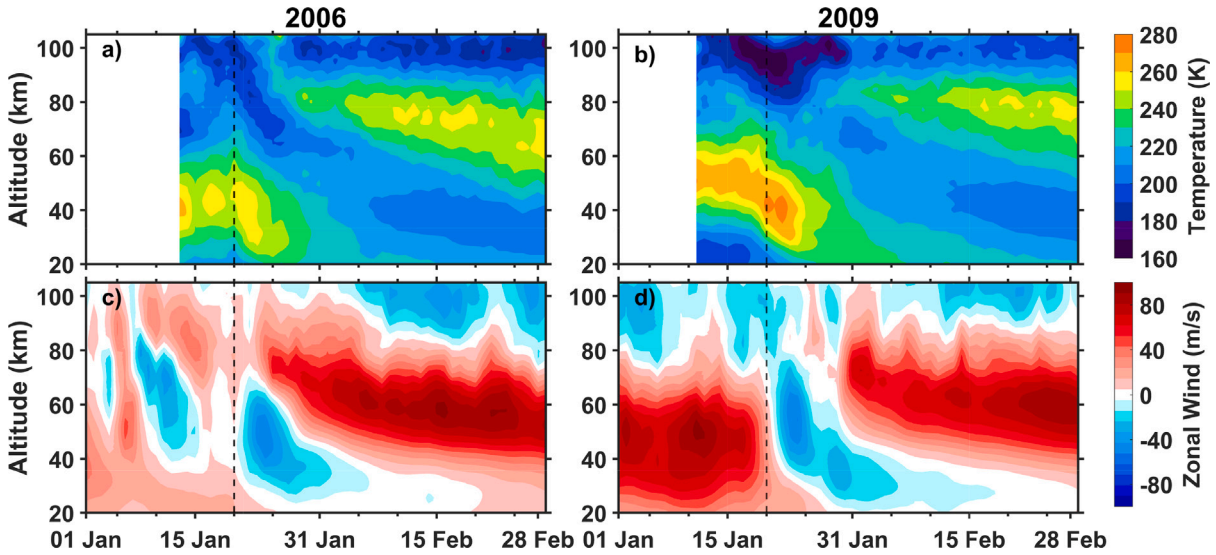

Fig. 1. Daily averaged zonal mean temperature (a–b) between 70° and 80° N derived from SABER observations in north viewing mode during (a) 2006 and (b) 2009 winters; zonal averaged daily zonal wind (c–d) at 60° N derived from WACCM-X modeled data during (c) 2006 and (d) 2009 winters. Positive values (red) indicate eastward winds, and the vertical lines indicate the SSW onset (zonal wind reversal at 1 hPa). (For interpretation of the references to color in this figure legend, the reader is referred to the web version of this article.)

The lower stratospheric temperature was already enhanced before the 2006 major SSW event and gradually starts to decrease when SABER starts measurements in the northern polar region.

The weakening of stratopause due to the SSW events, the subsequent formation of ES at an altitude above 80 km, and its gradual descent to its climatological altitude can be clearly seen for both the SSW-ES events in Fig. 1(a–b). It can also be seen from the figure that the polar mesospheric temperature decreases to its lowest value, corresponding very well in phase with the largest enhancement in the lower stratospheric temperature. The earlier onset of the SSW in the mesosphere compared to the stratosphere is clearly visible, as the temperature of the mesopause starts decreasing earlier with a descending mesopause altitude on January 20 (the vertical line indicating zonal wind reversal at 1 hPa) in both cases. The mesospheric cooling was stronger in the 2009 major SSW-ES event (40 K) in comparison to the 2006 event (20 K). The warming during the stratopause descent at the onset was also stronger in the 2009 event (50K) than the 2006 event (20 K). Despite similar defining characteristics, the magnitudes of the mesospheric cooling and stratospheric warming in the two SSW-ES events are different, which could be due to differences in the magnitude of residual circulation changes in both events.

The prominent feature of a major SSW, i.e., the wind reversal from eastward to westward, can be clearly noticed in Fig. 1(c–d). Although the WACCM-X modeled zonal winds have a strong westward bias in the high latitudes (Sassi et al., 2021), the lower stratospheric wind reversal can be seen as a prominent feature beginning on 20 January at 60° N and 10 hPa level (~ 30 km) for 2006 and 2009 SSW events, respectively. The weakening of strong circulation (eastward) before the SSW onset leading to a reversal from eastward (~ 100 km/s) to westward (~ 40 km/s) in the stratosphere can be noticed to occur during the peak SSW period. It can be seen that the zonal winds were reversed above 10 hPa level several days before the commencement of the SSW-ES in the winter of 2006, with enhanced lower stratospheric temperatures indicating a minor SSW event, but the intensification of westward winds occurred at the time of the SSW-ES onset. During the 2006 winter, the atmosphere began to recover from the minor SSW event around January 15, while the major SSW-ES began to develop on January 20.

The prevailing westward zonal mean winds in the mesosphere start to reverse much ahead of the lower stratospheric wind reversal. The zonal wind reversal in the lower mesosphere can be seen on January 20 of the 2006 and 2009 winters, which quickly descended into the lower stratosphere (on January 25). The early reversal of mesospheric winds has also been confirmed by Iida et al. (2014) and suggested that large-scale waves, generated by instabilities, cause the earlier wind reversal in the polar mesosphere during an SSW. However, the role of the lower atmospheric conditions prior to and during an SSW onset cannot be neglected (Kurihara et al., 2010). The upper mesospheric wind is completely reversed during the same time when the stratospheric eastward winds are reversed, and subsequently, we can see strong eastward winds in the upper mesospheric altitudes, particularly during the 2006 event. Meanwhile, the winds continued to be westward in the stratosphere until the eastward winds from mesospheric altitudes descended to the climatological polar stratopause altitude, coinciding with the reformation of the stratopause for the major SSW events represented in Fig. 1(a–b).

It is now widely accepted that upward and equatorward propagating planetary waves with large amplitudes break in the USLM and disturb the mean circulation (e.g., (Baldwin et al., 2021), Chandran et al. (2014), Matsuno (1971) and references therein). As the SSW event starts to unfold, resulting in the slowing down of stratospheric westerly winds, more eastward propagating gravity waves begin to saturate at the mesospheric altitudes, thus providing more eastward forcing (Liu and Roble, 2002). The westward gravity waves are limited by the anomalous stratospheric westward wind, and thus the eastward waves propagate to higher altitudes. The saturation of eastward propagating waves helps sustain the stratospheric temperature increase by facilitating more downwelling over the winter polar stratosphere. Due to the increased drag of eastward propagating gravity waves in the mesosphere, the downwelling can decrease and result in the cooling of the mesosphere and subsequent disappearance of the stratopause (Limpasuvan et al., 2016; Siskind et al., 2005), as seen inFig. 1.

After the SSW onset, due to the reversal of the stratospheric residual circulation, the westward forcing by the planetary waves dominates the eastward forcing by the gravity waves in the mesosphere, and this westward planetary wave drag drives the poleward and downward circulation (Limpasuvan et al., 2012). The downward circulation causes adiabatic heating and forms an elevated stratopause at the mesospheric altitudes (Chandran et al., 2014; Limpasuvan et al., 2016), modifying the thermal structure there. The mesospheric westward winds and cooling rapidly propagate downward due to enhanced dissipation of the

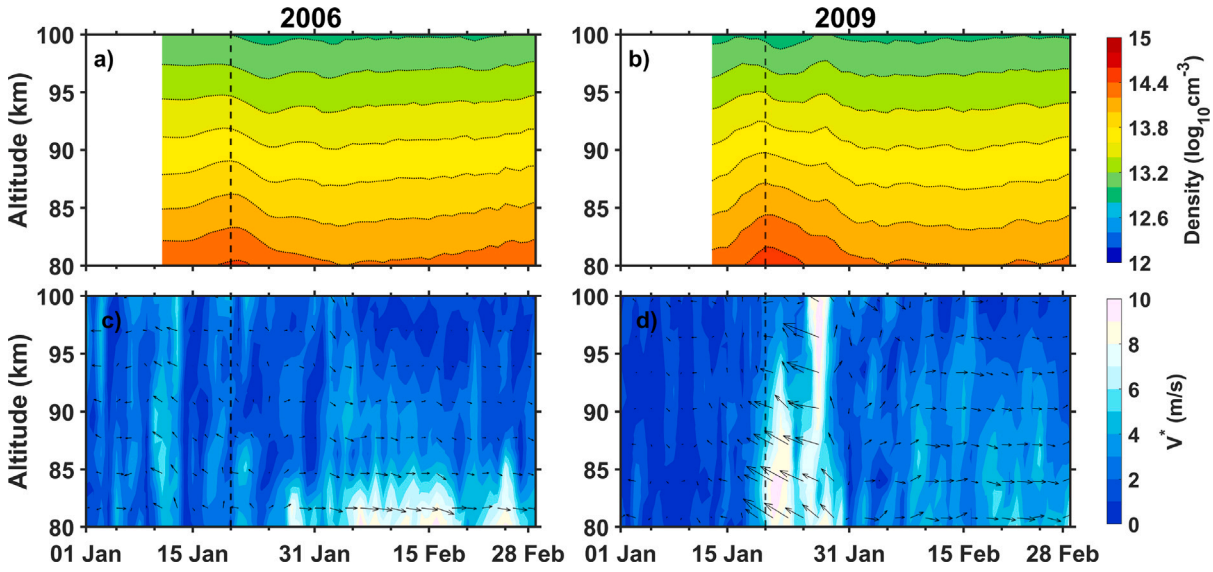

Fig. 2. Daily averaged zonal mean neutral density derived from SABER observations during (a) 2006 and (b) 2009 winters, zonal averaged daily meridional residual circulation derived from WACCM-X model data during (c) 2006 and (d) 2009 winters between 70° and 80° N. The arrows in the lower row indicate the directions, and colored contours show the magnitude of the meridional residual circulation. (For interpretation of the references to color in this figure legend, the reader is referred to the web version of this article.)

eastward propagating gravity waves in the upper mesosphere (Siskind et al., 2005). During the recovery phase of SSW, the reversed circulation decays quickly, followed by a pattern more characteristic of a typical winter. This wave-driven mean circulation in high latitude winters brings the ES to its climatological altitudes gradually (Limpasuvan et al., 2012). This change of wind has been shown to have profound significance in the polar mesospheric and stratospheric composition, and chemistry.

3.2. Effects of major SSW events on polar mesospheric neutral abundance

In line with the earlier discussion, it is clear that these events can have a strong bearing on the neutral abundances by means of temperature-dependent rate coefficients and/or due to the dynamical processes driven by these events. In order to further understand their effect on neutral densities, the daily averaged zonal mean atmospheric neutral density obtained from SABER (a–b) and the zonal averaged daily meridional circulation, V* (c–d) derived from WACCM-X output data between 70° and 80° N have been shown in Fig. 2 for these major events.

The magnitude of the meridional residual circulation (V*) is given by $V^* = \sqrt{v^{*2} + w^{*2}}$, where v^* and w^* are the meridional and vertical components of the residual circulation, and the vectors indicate the averaged (v, w) wind components. The meridional residual circulation with strong upward vertical wind is referred to as upward residual circulation, whereas the meridional residual circulation with strong downward vertical wind is denoted as downward residual circulation. From the figure, it can be noticed that the neutral density increases earlier in the polar upper mesosphere during the onset of the SSW event, coinciding with the decrease in the mesospheric temperature.

The large variation in density is observed at lower altitudes compared to higher altitudes in the mesosphere compared to their pre-SSW values. An increase of ~ 20% in the density at the onset and a ~ 30% decrease after the SSW compared to pre-SSW values have been observed below 90 km during the 2006 event. During the 2009 SSW event, ~ 70% density enhancement at the onset and ~ 20% density reduction after the SSW compared to pre-onset values have been observed below 90 km. The relative low density enhancements during the 2006 major SSW onset in comparison to the 2009 event could be due to the already increased density level felicitated by the 2006 minor SSW event. The increase in the neutral density can be due to the strong upward and equator-ward circulation at the SSW-ES onset, as seen in Fig. 2(c–d). In the MLT region, the upward residual circulation was stronger during a minor SSW event than during the major SSW event in January 2006, while the upward residual circulation was very strong during the 2009 major SSW, as seen in Fig. 2(c–d). Whereas, downward residual circulation was more intense after the 2006 event than the 2009 event. These changes in the residual circulation are attributed to be the main cause of the observed density variation during these events.

The denser air mass moves upward due to intensified upward circulation, supplementing neutral density in the MLT region, and leads to adiabatic cooling by means of expansion. The equator-ward and upward flow in the stratosphere can influence the westward gravity waves, which result in the earlier reversal of the mesospheric circulation and simultaneous mesospheric cooling associated with the upward motion (Liu and Roble, 2002; Smith-Johnsen et al., 2018). This cooling of the mesosphere further leads to a contraction of the atmosphere and an increase in the neutral density at the corresponding altitude of cooling in the upper mesosphere, followed by a decrease in density above it. Yamazaki et al. (2015) also reported a decrease in the thermospheric density during the SSW events. As the temperature starts increasing in the mesosphere with the ES formation due to downward circulation after the peak warming period, the neutral density starts decreasing due to the strong downward residual circulation. The downward residual circulation, driven by wave forcing in the recovery phase of the SSW events, brings less dense air mass from higher to lower altitudes, resulting in reduced density in the polar mesospheric region. It is apparent from the context above that the 2006 SSW-ES occurring with minor SSW affects neutral density less than the 2009 SSW-ES that occurs without minor SSW. This difference in response could be attributed to the displaced and split polar vortex during the 2006 and 2009 SSW events, respectively. The response of the displaced/split events needs to be investigated in detail, which is beyond the scope of our study as we employ the zonal mean approach to investigate the temporal variation during these events.

3.3. Effects of major SSW events on polar mesospheric NO radiative cooling

The above discussion underlines the role of SSW events in modulating the structure and energetics of the whole atmosphere in general and the stratosphere and mesosphere in particular. This large-scale temperature and compositional change can have a significant effect

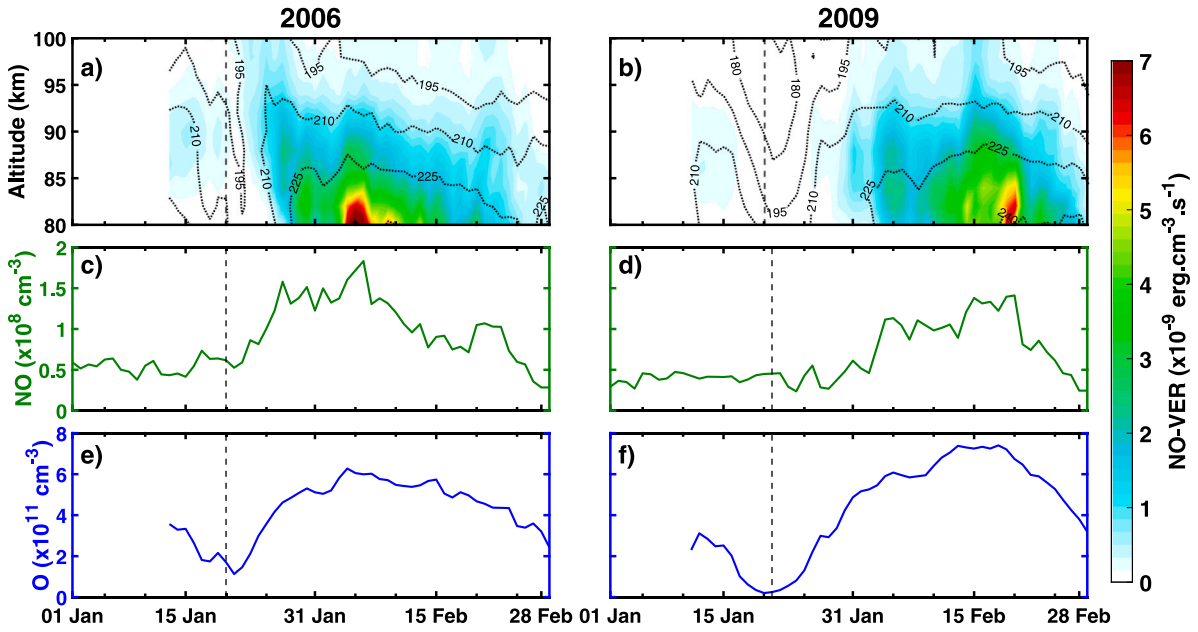

Fig. 3. Daily averaged zonal mean NO-VER (a–b), NO density derived from SCIAMACHY (c–d), and O density measured by SABER (e–f) between 70° and 80° N at MLT altitudes (80–100 km) during 2006 and 2009 SSW events, respectively. The dashed contour lines (a–b) indicate the temperature variations.

on the radiative emission processes and on the primary and secondary layers of ozone. The NO_x trace species is known to be responsible for balancing the ozone in the stratosphere (Lary, 1997; Solomon et al., 1982) and controlling the overall heat budget in the upper mesosphere and thermosphere (Mlynczak et al., 2005). As discussed earlier, the infrared radiative emission by NO at 5.3 μm plays a crucial role in cooling the upper mesosphere and lower thermosphere, particularly during a geomagnetic storm. Since the NO is vibrational IR-active, the NO present in the mesospheric altitudes is also highly sensitive to changes in temperature.

In addition to the temperature, the compositional changes in oxygen and nitrogen can also significantly influence the overall infrared energy output by NO. Thus, the key ingredients of NO chemistry and the radiative emission process are highly subjected to the effects induced in the atmosphere during the major SSW events. The availability of NO density from SCIAMACHY can help us gather information on the chemistry, dynamics, temperature, and wind structure in the MLT region. This effect on NO emission is presented in continuation with the earlier discussion. In order to obtain the magnitude of the NO radiative flux exciting from the mesosphere, the 5.3 μm volume emission rate (VER) for the NO molecule can be estimated (Khomich et al., 2008) by Eq. (1).

$$\text{NO–VER} = h\nu\left\{\frac{[\text{NO}]\times\left(\alpha_{\text{NO}_\text{O}}\times[\text{O}]+\alpha_{\text{NO}_{\text{O2}}}\times[\text{O}_2]+\alpha_{\text{NO}_{\text{N2}}}\times[\text{N}_2]\right)}{1+\left(\frac{\beta_{\text{NO}_\text{O}}\times[\text{O}]+\beta_{\text{NO}_{\text{O2}}}\times[\text{O}_2]+\beta_{\text{NO}_{\text{N2}}}\times[\text{N}_2]+\beta_{\text{NO}^+_{\text{O2}}}\times[\text{O}^+_2]}{A_{5.3}}\right)}\right\} \quad (1)$$

where $\alpha = \beta\ \exp(-h\nu/kT)$ are excitation rate coefficients ($\text{cm}^{-3}\text{s}^{-1}$) and
$\beta_{\text{NO}_\text{O}} = 4.2\times10^{-11}$ (Hwang et al., 2003),
$\beta_{\text{NO}_{\text{O2}}} = 2.4\times10^{-14}$ (Murphy et al., 1975),
$\beta_{\text{NO}_{\text{N2}}} = 1.7\times10^{-16}$ (Murphy et al., 1975),
$\beta_{\text{NO}^+_{\text{O2}}} = 4.4\times10^{-10}$ (Khomich et al., 2008)
are de-excitation rate coefficients ($\text{cm}^{-3}\text{s}^{-1}$) of NO molecule by the corresponding atoms, molecules, and ions. The quantities in brackets represent the corresponding concentrations (cm^{-3}), and the value of the Einstein coefficient $A_{5.3}$ is 13.38.

In Fig. 3, variation in the NO-VER calculated from SCIAMACHY-derived NO density and SABER-derived temperature (a,b), NO density (c–d), and O density (e–f), averaged daily between 70° and 80° N during the 2006 and 2009 winters, respectively, is shown.

Since major changes in NO-VER are seen between 80 and 90 km, the zonally averaged daily NO and O densities between these altitudes are shown, along with the NO-VER. There are uncertainties in the SABER observed NO-VER below 115 km (Mlynczak et al., 2021), therefore, the calculated NO-VER are employed, which have lower values than SABER derived NO-VER. These results are consistent with Mlynczak et al. (2021) indicating large values of SABER observed NO-VER.

The variability of NO-VER directly correlates with the changes in the thermal structure of the MLT region during SSW events. Hence, an understanding of the cooling pattern of the MLT region can be obtained from the calculated NO-VER during these major SSW events. The impact of the 2006 minor SSW cannot be seen on the NO-VER, NO, and O densities before the major SSW onset in the 2006 winter, as SABER starts measurements only after the recovery of the 2006 minor SSW in the northern polar region. It can be seen from Fig. 3(a–b) that at the SSW onset, i.e., when winds started to slow down, the NO-VER decreased vaguely from its pre-SSW values following the decrease in upper mesospheric temperature. It can also be seen from the figure that the NO-VER reaches its lowest value when the zonal wind reversal occurs, coinciding with the minimum values of O (Fig. 3.e–3.f) and temperature in the mesosphere during these events. These changes in temperature and O density can influence the radiative emissions by NO, since the magnitude of NO-VER is proportional to the rate of collisional excitation of NO into the vibrationally excited state NO(v=1), as shown in R1.

$$\text{NO}(v=0)+\text{O} \xrightarrow{C_{01}} \text{NO}(v=1)+\text{O} \quad (\text{R1})$$

The rate of collisional excitation $C_{01} = k_1[O]e^{-2700/T}; k_1 = 4.2\times10^{-11}$ cm^3s^{-1} in the MLT region strongly depends on the temperature and O (Sharma et al., 1998; Mlynczak et al., 2003).

The wind reversal changes the gravity wave filtering, thereby changing the circulation in the upper mesosphere from poleward/downward to equatorward/upward. This change in the circulation results in a net depletion in the O density at the mesospheric altitudes (Liu and Roble, 2002; Medvedeva et al., 2019; Shepherd et al., 2010). The decreased O and low temperature reduce the rate of collision excitation of NO and, therefore, less NO-VER during the SSW onset. As discussed above, before the peak warming period in the stratosphere, the reversed circulation causes a decrease in temperature, NO, and O density in

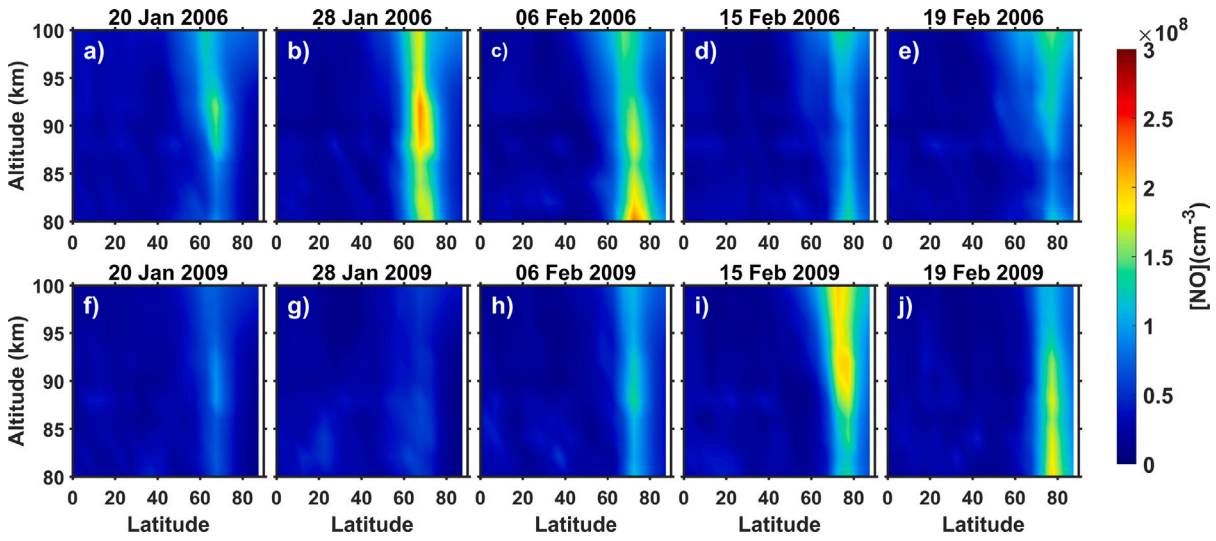

Fig. 4. Zonal mean NO density derived from SCIAMACHY between 0° and 90° N in the MLT region during 2006 (upper row) and 2009 (lower row) SSW events, respectively.

the mesosphere. The depletion in NO density is negligible while O reduced by about 200% and 250% in comparison of pre-onset values in the 2006 and 2009 events, respectively (Fig. 3.c–3.f). The values of these three parameters (temperature, O, and NO) during the peak warming period in the stratosphere have not recovered to their pre-SSW values at mesospheric altitudes, therefore resulting in marginally reduced NO-VER during peak warming periods.

The recovery phase of SSW is accompanied by an increase in temperature, NO, and O in the polar mesosphere. From Fig. 3, the increase in NO-VER following the variation of other parameters is very straightforward. The 2009 event was extended, therefore showing a delayed enhancement of NO-VER, NO, and O densities during its recovery phase in comparison to the 2006 event. In the recovery phase, NO-VER enhanced ~ 400% and ~ 500% to the pre-onset values during the 2006 and 2009 SSW events, respectively. The NO-VER enhancement appeared to follow the increased temperature pattern during ES formation in the recovery phase of both major events, but the sharp enhancements were observed during rapid NO and O increments. The enhancement in NO-VER can be attributed to an increase in temperature, NO, and O due to the downward flow of lower thermospheric air into the mesosphere (Liu and Roble, 2002; Shepherd et al., 2010) (Fig. 2.c–2.d). It is clear from Fig. 3(c–f) that in the recovery phase of both the major SSW events, the NO density enhanced ~ 300% to its pre-onset values, whereas the O density enhanced ~ 250% and ~ 300% to its pre-SSW values during the 2006 and 2009 events, respectively. This abundance of NO, O, and other trace species has been created by the enhanced descent of polar thermospheric air into the mesosphere (Bailey et al., 2014; Pérot and Orsolini, 2021; Randall et al., 2006; Siskind et al., 2007; Wang et al., 2019).

The descent of NO abundant from the thermosphere into the mesosphere over the polar region following the ES formation can be seen in Fig. 4.

The narrow maxima confined near 70° N is a result of NO production by energetic electron precipitation along the auroral latitudes. During the 2006 event, the vertical transport of the NO-rich air occurred very quickly after the SSW event (Fig. 4.b &c), when the downward residual circulation established at the mesospheric altitudes. Since the 2009 SSW-ES event was more prolonged, the delayed vertical transport eventuated (4.h–4.i) when the more characteristic wintertime circulation has re-established over the polar mesosphere. Our results are consistent with earlier studies (Bailey et al., 2014; Pérot and Orsolini, 2021; Randall et al., 2006) indicating downward transport of NO into the mesosphere from the thermosphere.

To understand the relative importance of the temperature NO and O on the NO radiative emission in the MLT, a sensitivity analysis is performed. As discussed earlier, NO radiative emission is strongly dependent on temperature, changes in the concentration of NO, and O. Hence, an analysis of NO-VER variation independently with these parameters at mesospheric altitudes (80–90 km) during these SSW events is presented in Fig. 5.

The variation of NO-VER with any particular species at mesospheric altitudes (80–90 km) is analyzed by taking the mean of the pre-SSW values of other species. The SCIAMACHY measurements of NO density support the modeled variation of NO-VER very well, also indicating that the role of increased NO abundance and temperature is more critical in the overall infrared flux radiating out, particularly in the recovery phase of both the SSW-ES events. During the SSW onset, the reduced temperature and O density are responsible for the observed decrease in NO-VER (Fig. 5.a–5.f).

It is evident from the figure that temperature enhancement during ES formation plays a very crucial role in the NO-VER variations; however, the contribution of enhanced NO abundance appears to be larger (Fig. 5.c–d) than the temperature (Fig. 5.a–5.b). The role of O was limited during ES formation (Fig. 5.e–5.f) in both events. This is consistent with Bharti et al. (2018), suggesting the important role of NO density enhancement in the NO radiative cooling. During the ES formation in the polar mesosphere, the increased temperature facilitates higher collisional excitation of NO, resulting in a higher NO-VER. However, this variation is prominent during the downward circulation when ES forms at mesospheric altitudes. This variation suggests the relative importance of trace species and temperature, and the role of mesospheric dynamics on the overall infrared emission.

3.4. Impact of major SSW events on polar secondary ozone layer

Ozone, being a very important trace species, can show considerable variation during SSW events (Smith et al., 2009, 2014; Smith-Johnsen et al., 2018). As mentioned earlier, the availability of O and H can significantly affect the overall abundance of O_3 at the secondary peak. The decrease in stratospheric O_3 can be ascribed to the strong NO_x descent during SSW events occurring early enough in the winter period (Randall et al., 2009; Rozanov et al., 2005). Therefore, various aspects related to NO in the middle and upper atmosphere and its interrelation with the O_3 species need a detailed analysis. The daily averaged zonal mean night-time O_3 density between 70° and 80° N, along with temperature, H, and O density, obtained from night-time

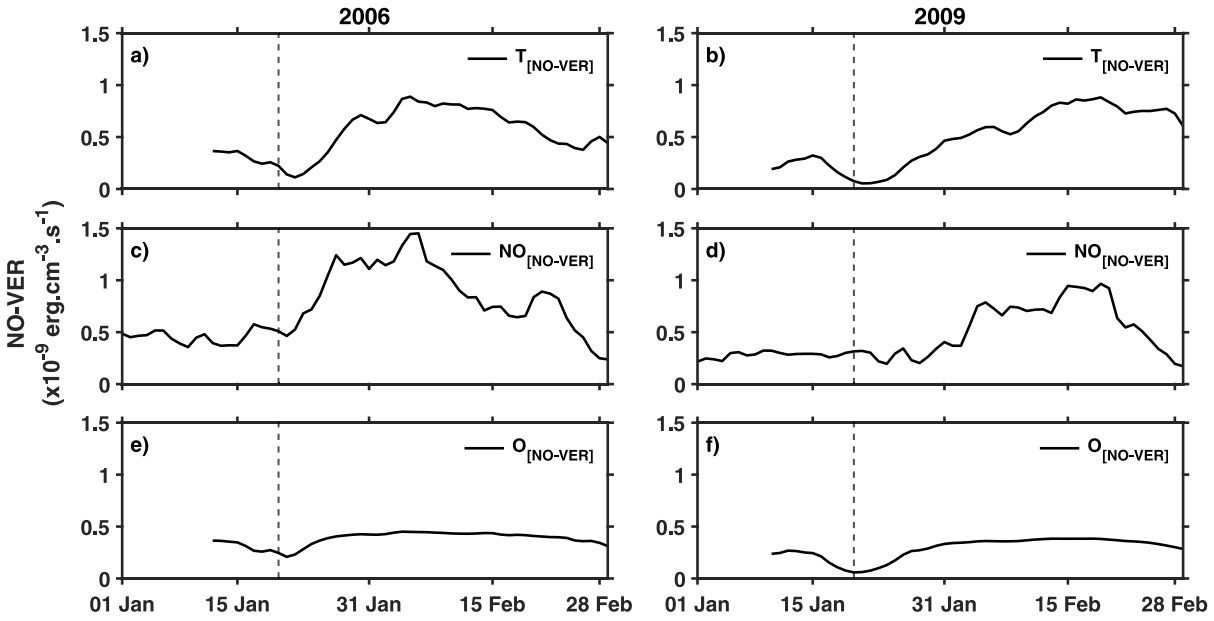

Fig. 5. Daily averaged zonal mean NO-VER variation due to temperature (a–b), NO density (c–d), and O density (e–f) between 70° and 80° N at mesospheric altitudes (80–90 km) during 2006 and 2009 SSW events, respectively.

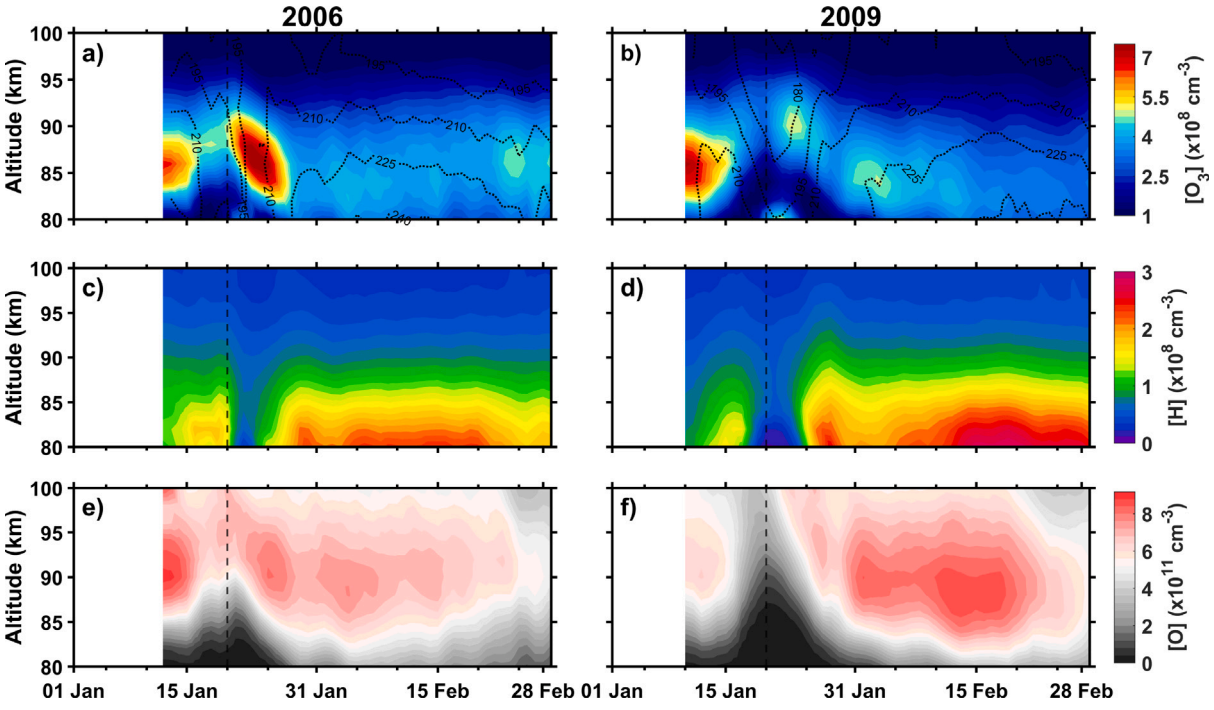

Fig. 6. Variations in daily averaged zonal mean night-time O_3 density (a–b), H density (c–d), and O density (e–f) derived from night-time SABER measurements between 70° and 80° N during 2006 and 2009 SSW events, respectively. The dashed contour lines indicate the temperature variation.

SABER measurements during the 2006 and 2009 major SSW events, is shown in Fig. 6.

The impact of the 2006 minor SSW cannot be seen in the O_3, H and O densities before the 2006 major SSW-ES onset due to the delayed measurements by SABER in north viewing mode. It is evident from Fig. 6(a–b) that just before the onset, there is a ~ 20% and ~ 40% decrease in the night-time secondary O_3 in comparison to their pre-onset values during the 2006 and 2009 events, respectively. This decrease coincides with a drop in temperature when the residual circulation starts to slow down in the polar mesosphere. This decrease in O_3 is also accompanied by a rapid decrease of ~ 35% and ~ 65% in O density and a sudden enhancement of ~ 5% and ~ 10% in H density compared to their pre-onset values (Fig. 6(c–f)), just before the onset of 2006 and 2009 SSW events, respectively. This observed variation of trace species can be the main reason for the changes in O_3 as seen in Fig. 6(a, b). The O reduction and H enhancement are large, which leads to a large depletion in the secondary O_3 peak density prior to the 2009 SSW onset. Moreover, the peak O_3 density also shifts about 3–4 km upward during the onset phase of these major SSW events. This upward displacement of the secondary O_3 peak further confirms the upward residual circulation during the SSW onset (Fig. 6(c–d)), consistent with the earlier discussion.

It can be seen from Fig. 6(a) that the secondary peak O_3 density was suddenly enhanced by ~ 25% coinciding with ~ 40% reduction in H and ~ 10% depletion in O densities from their pre-SSW values. This sudden increase is consistent with the earlier reports suggesting a short-duration change in the secondary O_3 due to reduced temperature and O (Smith-Johnsen et al., 2018; Tweedy et al., 2013). Whereas, during the 2009 event, the peak O_3 density decreased by ~ 15%, accompanied by about a ~ 35% decrease in H and a ~ 40% reduction in O densities after the onset of the 2009 event. During the recovery phase of both the SSW events, the peak O_3 altitude descended (3–4 km) to the altitude of peak H. As the elevated peak O_3 altitude descends, ~ 35% and ~ 50% depletion in O_3 peak density is noticed in comparison to its pre-onset values after the 2006 and 2009 SSW events, respectively. At the same time, ~ 35% and ~ 50% enhancement in H was also observed at mesospheric attitudes during the 2006 and 2009 events, respectively. A depletion of ~ 20% and an increase of ~ 40% in O density were observed during the 2006 and 2009 events in comparison to pre-SSW values. Thus, it is evident from the figure (Fig. 6.c–6.d) that enhanced abundance of H and low availability of O during the recovery phase of SSW can cause more O_3 depletion at its peak altitude. As we know, hydrogen is a very efficient sink for the ozone density. This descent of the peak O_3 layer has caused an effective quenching of the available O_3. This enhanced destruction of secondary O_3 is stronger during the 2009 event due to the larger availability of H at secondary O_3 peak altitude in the recovery phase of SSW (10 February onward). An earlier report by Tweedy et al. (2013) has mentioned the enhanced downward transport of H but did not consider the consequences that arise following the descent of peak O_3 altitude. The role of O during these events appears to be strengthening the O_3 density and has been investigated further.

The production and destruction processes of night-time O_3 are temperature and oxygen density dependent, and higher O_3 concentrations are generally associated with colder temperatures in the MLT region (Smith and Marsh, 2005). During the formation of ES, the supplemented temperature changes can also destroy O_3 in the MLT region. Some of the earlier studies (Kvissel et al., 2012; Salmi et al., 2011) also reported the reduced amplitude of secondary O_3 during the ES formation. It is to be noted that the 2009 SSW event was more prolonged among these, resulting in the largest displacement of peak altitude and density of the secondary O_3 layer during the main and recovery phases of the SSW. Furthermore, albeit having similar defining characteristics, the 2009 SSW-ES event, which occurred solely, seems to impact the trace species abundance in the MLT region more than the 2006 SSW-ES event, which preceded with a minor SSW.

From the earlier discussion, it can be contended that the O_3 variation is influenced by changes in temperature and other trace species. Therefore, the correlations between O_3, temperature, and other trace species at the secondary O_3 peak altitude (84–94 km) in the polar region (where major changes are observed) are shown in Fig. 7.

All the values of the trace species are night-time daily averages, except for NO density, since NO observations are derived from the morning and evening time occultation-measurement profiles from SCIAMACHY. Moreover, NO densities are assumed to be same in both day and night due to their increased lifetime in the polar winters. It is clear from the figure that O_3 and temperature are anti-correlated with a correlation coefficient of −0.585 and −0.401 during the 2006 and 2009 SSW-ES events, respectively. A similar anti-correlation can also be seen between O_3 and H during both the SSW-ES events. However, the anti-correlation was smaller during the 2009 event (−0.517) in comparison to the 2006 event (−0.891). There is also a weak anti-correlation between O_3 and O densities during both the SSW-ES events, but the correlation factor is slightly lower in the case of the 2006 event. Although the role of NO in the destruction of O_3 above 80 km is not clearly established, the O_3 and NO densities are anti-correlated during both the SSW-ES events, and this anti-correlation is similar in both events, suggesting an interaction between O_3 and NO in the MLT region. These results are slightly different from those presented in Tweedy et al. (2013), which could be due to the fact that the present study is mainly based on observational datasets and the target altitude and time of observation being different.

In order to understand the contribution of different trace species to the observed variability of peak O_3 density, a sensitivity analysis at the secondary O_3 peak altitude (84–94 km) is presented in Fig. 8. The variation due to NO fluctuations is also introduced to the secondary O_3 maximum equation (Smith and Marsh, 2005) (Eq. (2)). Because of the increased lifetime during the nighttime, NO can also be considered as a potential candidate for the catalytic destruction of O_3 in the middle atmosphere.

$$[O_3] = \frac{k_1[O][O_2]\rho}{k_2[O] + k_3[H] + k_4[NO]}, \tag{2}$$

Where, k_1, k_2, k_3, k_4 are the temperature-dependent reaction rate coefficients.

$$k_1 = 6.0 \times 10^{-34}\left(\frac{300}{T}\right)^{2.4},$$

(Sander et al., 2006),

$$k_2 = 8.0 \times 10^{-12} exp\left(\frac{-2060}{T}\right),$$

(Sander et al., 2006),

$$k_3 = 1.1 \times 10^{-10} exp\left(\frac{-470}{T}\right),$$

(Sander et al., 2006),

$$k_4 = 1.4 \times 10^{-12} exp\left(\frac{-1310}{T}\right)$$

(Schofield, 1967)

Variation in O_3 density with selected parameter at O_3 peak altitude (84–94 km) is studied by taking the pre-SSW mean values of the remaining parameters. Although the calculated O_3 density from the secondary O_3 maximum equation is 1.5–2 times larger than SABER measured values during SSW onset, the variation pattern is similar to the observation. The influence of temperature on the net O_3 is very clear from the figure during both events. The variation in temperature during the entire event is very well exhibited by the calculated O_3 density represented by the black line. The blue dashed line indicates the SABER observed O_3 density in all panels of Fig. 8. The primary factor in the abrupt increase in O_3 density following the onset appears to be the low temperature during mesospheric cooling (Fig. 8.c–8.d). However, the reduced H during onset (Fig. 8.g–8.h) also contributes to the sudden enhancement in the secondary O_3 peak density, primarily due to decreased destruction.

From Fig. 8(f), it can be seen that the reduced O density during the 2009 event led to a larger depletion in O_3 density in comparison to the 2006 event. As expected, the NO does not seem to contribute to any change in O_3 density at these altitudes during both events (Fig. 8.i–8.j). The reduced availability of H in combination with the low temperature during the ascending O_3 peak altitude resulted in sudden O_3 enhancement during SSW onset. However, the availability of O seems to limit this enhancement. Although, during the 2009 SSW onset, a significant decrease in temperature and H density ideally should cause a large O_3 enhancement similar to the 2006 event, but a substantial depletion in O density resulted in curtailed O_3 density as observed during the 2009 SSW onset (Fig. 8.b). Despite large decrease in H density and in temperature during the 2009 SSW onset, the decrease in O_3 is larger compared to the 2006 event. This might occur as a result of the 2009 event's considerable O density reduction. After the onset, contribution of O dominates over temperature and H in the O_3 peak density variation (Fig. 8.e–8.f), and it is large during the 2009 SSW. At the descended O_3 peak altitude during ES formation, the availability of O counteracts the O_3 destruction by the increased H and temperature.

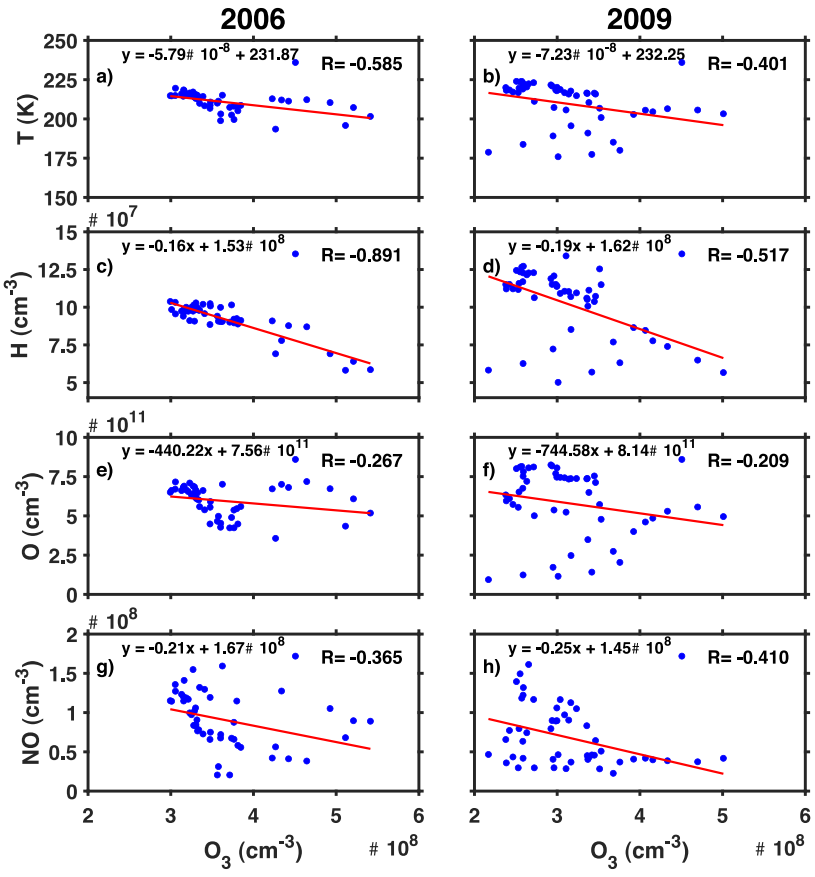

Fig. 7. Correlation between daily averaged zonal mean O_3 and temperature (a–b), H (c–d), O (e–f), NO (g–h) at the secondary O_3 peak altitude (84–94 km) between 70° and 80° N during the 2006 and 2009 major SSW events, respectively.

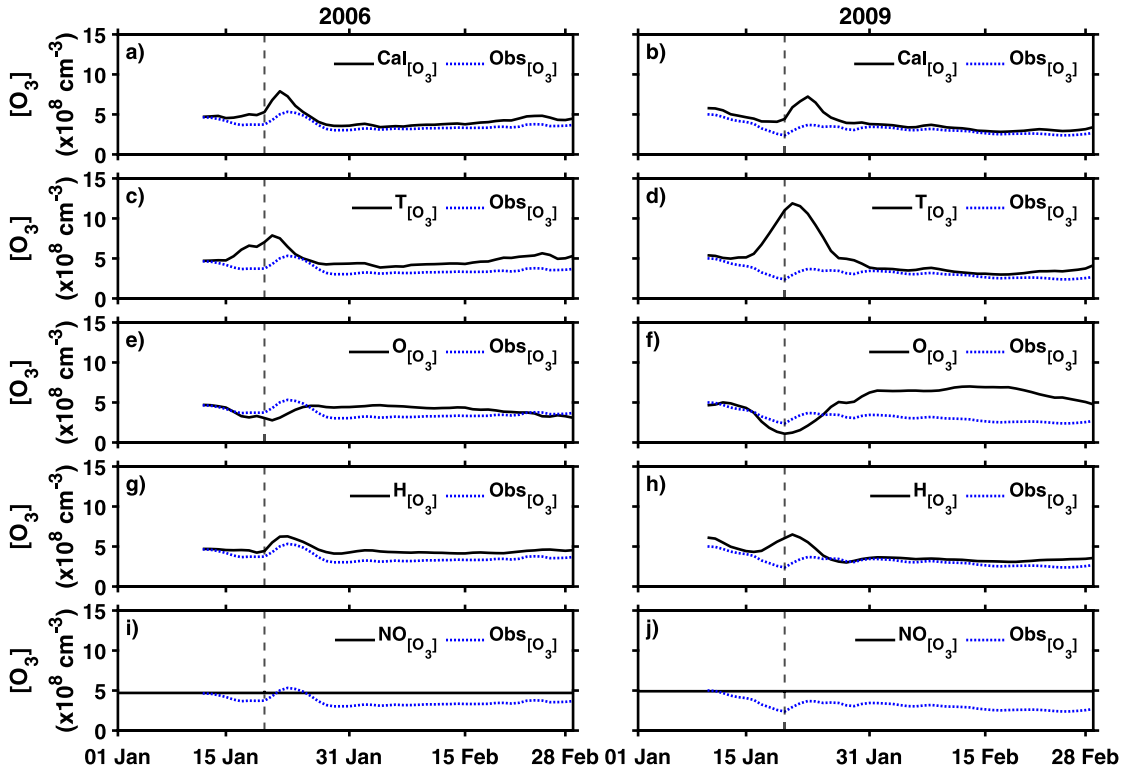

Fig. 8. Daily averaged zonal mean night-time calculated O_3 variation (black) (a–b) due to temperature (c–d), O density (e–f), H density (g–h), and NO density (i–j) between 70° and 80° N at the secondary O_3 peak altitude (84–94 km) during 2006 and 2009 SSW events, respectively. The blue dotted lines in all panels indicate the SABER observed O_3 density. (For interpretation of the references to color in this figure legend, the reader is referred to the web version of this article.)

Therefore, we conclude that the availability of O is very crucial for the observed variability of secondary O_3 density.

The explanation above makes clear that the MLT region was significantly impacted by the 2009 major SSW, which was more severe than the 2006 major SSW. The measurements of SCIAMACHY and SABER used in the present study indicate that during the ES formation, both the NO density and O_3 density are anti-correlated in the mesosphere, suggesting a similar catalytic destruction as seen in the stratosphere. But in further analysis and based on earlier studies (Kvissel et al., 2012; Smith and Marsh, 2005), it can be said that the O_3 and NO are both similarly influenced by the transport and temperature changes, and the role of chemical interaction between them is less likely. However, the secondary O_3 peak is more influenced by the availability of O than the temperature and H density variations. Therefore, it can be concluded that the variation in secondary O_3 peak can be attributed to increased production due to low temperature and large availability of O, and loss due to the enhanced temperature and less abundant O. However, we cannot neglect the effects of change in H on the O_3 variation (Smith-Johnsen et al., 2018; Tweedy et al., 2013; Damiani et al., 2010; Salmi et al., 2011). The differential role of temperature during the main and recovery phase in combination with the neutral species further adds to the observed variability in NO-VER and O_3.

4. Summary

In this study, we present an analysis of the variability in temperature and vertically transported trace species, and their consequences on the radiative emission by NO at 5.3 μm and secondary O_3 maximum in MLT region, during two major SSW-ES events : the 2006 SSW-ES happening after a minor SSW, and the 2009 SSW-ES event. The defining features of a major SSW such as zonal wind reversal and temperature enhancement by several tens of Kelvin in the stratosphere are similar in both the events and are clearly established using the SABER measurements and WACCM-X output data. The altered residual circulation, due to change in gravity wave filtering, causes the neutral densities in mesospheric altitude to increase and decrease during the initial and recovery phases of SSW, respectively. The upward residual circulation also depletes the O density and temperature in the mesosphere causing the net NO-VER to decrease during the mesospheric cooling period, and subsequently the intense downwelling of NO during the formation of ES causes more production of vibrationally excited NO that resulted in the net enhancement in NO-VER. Since NO-VER is a measure of radiative cooling, the large enhancement in its values indicates the increased cooling in the MLT region when ES forms at the mesospheric altitudes.

Despite having similar defining features, the secondary O_3 layer exhibits differential response to both the events. The secondary O_3 density is found to be decreasing during the initial phase of SSW due to the low temperature and low availability of O at its peak altitude. A sudden enhancement in the peak density and altitude of the secondary O_3 is caused by the variations in availability of O and H, and reduced temperature which is facilitated by the residual circulation change. Based on this analysis it is concluded that the sole 2009 SSW-ES event impacted the trace species abundance in MLT region to a greater extent compared to the 2006 SSW-ES event preceding a minor SSW event, in its initial and recovery phases. In other words, being an intense dynamic event, the 2009 SSW influences the MLT region strongly.

Despite a clear anti-correlation between O_3 and NO, the net effect of NO on O_3 variability is negligible. This anti-correlation during the SSW-ES may not be directly inferred to a similar chemical scheme of catalytic destruction of O_3 by NO seen in the stratosphere, but needs a more detailed study, particularly during enhanced mesospheric temperatures. The state of the polar vortex (displacement and splitting) can also influence the thermal structure and transport of trace species, which should be investigated further.

CRediT authorship contribution statement

Akash Kumar: Formal analysis, Investigation, Methodology, Software, Validation, Visualization, Writing – original draft, Writing – review & editing. **M.V. Sunil Krishna:** Conceptualization, Formal analysis, Funding acquisition, Investigation, Methodology, Project administration, Software, Supervision, Validation, Visualization, Writing – original draft, Writing – review & editing. **Alok Kumar Ranjan:** Formal analysis, Writing – original draft, Writing – review & editing. **Stefan Bender:** Data curation, Writing – original draft, Writing – review & editing. **Miriam Sinnhuber:** Data curation, Writing – original draft, Writing – review & editing. **Sumanta Sarkhel:** Funding acquisition, Writing – original draft, Writing – review & editing.

Declaration of competing interest

The authors declare that they have no known competing financial interests or personal relationships that could have appeared to influence the work reported in this paper.

Data availability

Data will be made available on request.

Acknowledgments

Authors acknowledge TIMED-SABER instrument, algorithm, and data processing teams for providing free access to the SABER dataset, available on the webpage: http://saber.gats-inc.com/data.php. Authors also thank the ENVISET/SCIAMACHY teams for providing the data obtained from https://zenodo.org/record/1009078 that are used in this study. The online-run facility for NRLMSISE-00 and IRI-2016 models are also available at https://ccmc.gsfc.nasa.gov/. We sincerely thank the WACCM-X team for providing free-run data of SD-WACCM-X that is available on the webpage: https://www.earthsystemgrid.org/dataset/ucar.cgd.ccsm4.SD-WACCM-X_v2.1.html. One of the authors, Akash Kumar, also thanks the DST-SERB, and Ministry of Education, Government of India for the financial support. The results presented in this paper are out of the DST-SERB, India funded research project (EMR/2017/005188).

References

Bailey, S., Thurairajah, B., Randall, C., Holt, L., Siskind, D., Harvey, V., Venkataramani, K., Hervig, M., Rong, P., Russell, J., 2014. A multi tracer analysis of thermosphere to stratosphere descent triggered by the 2013 Stratospheric Sudden Warming. Geophys. Res. Lett. 41 (14), 5216–5222. http://dx.doi.org/10.1002/2014GL059860.

Baldwin, M.P., Ayarzagüena, B., Birner, T., Butchart, N., Butler, A.H., Charlton-Perez, A.J., Domeisen, D.I., Garfinkel, C.I., Garny, H., Gerber, E.P., et al., 2021. Sudden stratospheric warmings. Rev. Geophys. 59 (1), http://dx.doi.org/10.1029/2020RG000708, e2020RG000708.

Barth, C.A., 1992. Nitric oxide in the lower thermosphere. Planet. Space Sci. 40 (2–3), 315–336. http://dx.doi.org/10.1016/0032-0633(92)90067-X.

Bender, S., Sinnhuber, M., Burrows, J.P., Langowski, M., 2017a. Nitric Oxide (NO) Data Set (60–160 Km) from SCIAMACHY Nominal Limb Scans. Zenodo, http://dx.doi.org/10.5281/zenodo.1009078, [Dataset].

Bender, S., Sinnhuber, M., Langowski, M., Burrows, J.P., 2017b. Retrieval of nitric oxide in the mesosphere from SCIAMACHY nominal limb spectra. Atmos. Meas. Tech. 10 (1), 209–220. http://dx.doi.org/10.5194/amt-10-209-2017.

Bharti, G., Sunil Krishna, M., Bag, T., Jain, P., 2018. Storm time variation of radiative cooling by nitric oxide as observed by TIMED-SABER and GUVI. J. Geophys. Res. Space Phys. 123 (2), 1500–1514. http://dx.doi.org/10.1002/2017JA024576.

Bovensmann, H., Burrows, J., Buchwitz, M., Frerick, J., Noel, S., Rozanov, V., Chance, K., Goede, A., 1999. SCIAMACHY: Mission objectives and measurement modes. J. Atmos. Sci. 56 (2), 127–150. http://dx.doi.org/10.1175/1520-0469(1999)056<0127:SMOAMM>E2.0.CO;2.

Burrows, J., Hölzle, E., Goede, A., Visser, H., Fricke, W., 1995. SCIAMACHY—Scanning imaging absorption spectrometer for atmospheric chartography. Acta Astronaut. 35 (7), 445–451. http://dx.doi.org/10.1016/0094-5765(94)00278-T.

Butler, A.H., Gerber, E.P., 2018. Optimizing the definition of a sudden stratospheric warming. J. Clim. 31 (6), 2337–2344. http://dx.doi.org/10.1175/JCLI-D-17-0648.1.

Butler, A.H., Seidel, D.J., Hardiman, S.C., Butchart, N., Birner, T., Match, A., 2015. Defining sudden stratospheric warmings. Bull. Am. Meteorol. Soc. 96 (11), 1913–1928. http://dx.doi.org/10.1175/BAMS-D-13-00173.1.

Chandran, A., Collins, R., Harvey, V., 2014. Stratosphere-mesosphere coupling during stratospheric sudden warming events. Adv. Space Res. 53 (9), 1265–1289. http://dx.doi.org/10.1016/j.asr.2014.02.005.

Charlton, A.J., Polvani, L.M., 2007. A new look at stratospheric sudden warmings. Part I: Climatology and modeling benchmarks. J. Clim. 20 (3), 449–469. http://dx.doi.org/10.1175/JCLI3996.1.

Charney, J.G., Drazin, P.G., 1990. Propagation of planetary-scale disturbances from the lower into the upper atmosphere. In: The Atmosphere—A Challenge. Springer, pp. 295–321. http://dx.doi.org/10.1007/978-1-944970-35-2_17.

Damiani, A., Storini, M., Santee, M., Wang, S., 2010. Variability of the nighttime OH layer and mesospheric ozone at high latitudes during northern winter: influence of meteorology. Atmos. Chem. Phys. 10 (21), 10291–10303. http://dx.doi.org/10.5194/acp-10-10291-2010.

De Grandpré, J., Beagley, S., Fomichev, V., Griffioen, E., McConnell, J., Medvedev, A., Shepherd, T., 2000. Ozone climatology using interactive chemistry: Results from the Canadian Middle Atmosphere Model. J. Geophys. Res.: Atmos. 105 (D21), 26475–26491. http://dx.doi.org/10.1029/2000JD900427.

de la Cámara, A., Albers, J.R., Birner, T., Garcia, R.R., Hitchcock, P., Kinnison, D.E., Smith, A.K., 2017. Sensitivity of sudden stratospheric warmings to previous stratospheric conditions. J. Atmos. Sci. 74 (9), 2857–2877. http://dx.doi.org/10.1175/JAS-D-17-0136.1.

Garcia, R.R., Smith, A.K., Kinnison, D.E., de la Cámara, Á., Murphy, D.J., 2017. Modification of the gravity wave parameterization in the Whole Atmosphere Community Climate Model: Motivation and results. J. Atmos. Sci. 74 (1), 275–291. http://dx.doi.org/10.1175/JAS-D-16-0104.1.

Goncharenko, L., Coster, A., Chau, J., Valladares, C., 2010. Impact of sudden stratospheric warmings on equatorial ionization anomaly. J. Geophys. Res. Space Phys. 115 (A10), http://dx.doi.org/10.1029/2010JA015400.

Gong, Y., Xue, J., Ma, Z., Zhang, S., Zhou, Q., Huang, C., Huang, K., Yu, Y., Li, G., 2021. Strong quarterdiurnal tides in the mesosphere and lower thermosphere during the 2019 Arctic sudden stratospheric warming over Mohe, China. J. Geophys. Res. Space Phys. 126 (10), http://dx.doi.org/10.1029/2020JA029066, e2020JA029066.

Gong, Y., Zhou, Q., Zhang, S., Aponte, N., Sulzer, M., 2016. An incoherent scatter radar study of the midnight temperature maximum that occurred at Arecibo during a sudden stratospheric warming event in January 2010. J. Geophys. Res. Space Phys. 121 (6), 5571–5578. http://dx.doi.org/10.1002/2016JA022439.

Holt, L.A., Randall, C.E., Peck, E.D., Marsh, D.R., Smith, A.K., Harvey, V.L., 2013. The influence of major sudden stratospheric warming and elevated stratopause events on the effects of energetic particle precipitation in WACCM. J. Geophys. Res.: Atmos. 118 (20), 11–636. http://dx.doi.org/10.1002/2013JD020294.

Holton, J.R., 1983. The influence of gravity wave breaking on the general circulation of the middle atmosphere. J. Atmos. Sci. 40 (10), 2497–2507. http://dx.doi.org/10.1175/1520-0469(1983)040<2497:TIOGWB>2.0.CO;2.

Hwang, E.S., Castle, K.J., Dodd, J.A., 2003. Vibrational relaxation of NO (v=1) by oxygen atoms between 295 and 825 K. J. Geophys. Res. Space Phys. 108 (A3), http://dx.doi.org/10.1029/2002JA009688.

Iida, C., Hirooka, T., Eguchi, N., 2014. Circulation changes in the stratosphere and mesosphere during the stratospheric sudden warming event in January 2009. J. Geophys. Res.: Atmos. 119 (12), 7104–7115. http://dx.doi.org/10.1002/2013JD021252.

Khomich, V.Y., Semenov, A.I., Shefov, N.N., 2008. Airglow as an Indicator of Upper Atmospheric Structure and Dynamics. Springer Science & Business Media, http://dx.doi.org/10.1007/978-3-540-75833-4.

Kockarts, G., 1980. Nitric oxide cooling in the terrestrial thermosphere. Geophys. Res. Lett. 7 (2), 137–140. http://dx.doi.org/10.1029/GL007i002p00137.

Kodera, K., Mukougawa, H., Maury, P., Ueda, M., Claud, C., 2016. Absorbing and reflecting sudden stratospheric warming events and their relationship with tropospheric circulation. J. Geophys. Res.: Atmos. 121 (1), 80–94. http://dx.doi.org/10.1002/2015JD023359.

Koushik, N., Kumar, K.K., Ramkumar, G., Subrahmanyam, K., 2018. Response of equatorial and low latitude mesosphere lower thermospheric dynamics to the northern hemispheric sudden stratospheric warming events. J. Atmos. Sol.-Terr. Phys. 169, 66–77. http://dx.doi.org/10.1016/j.jastp.2018.01.021.

Kurihara, J., Ogawa, Y., Oyama, S., Nozawa, S., Tsutsumi, M., Hall, C., Tomikawa, Y., Fujii, R., 2010. Links between a stratospheric sudden warming and thermal structures and dynamics in the high-latitude mesosphere, lower thermosphere, and ionosphere. Geophys. Res. Lett. 37 (13), http://dx.doi.org/10.1029/2010GL043643.

Kvissel, O.K., Orsolini, Y.J., Stordal, F., Limpasuvan, V., Richter, J., Marsh, D.R., 2012. Mesospheric intrusion and anomalous chemistry during and after a major stratospheric sudden warming. J. Atmos. Sol.-Terr. Phys. 78, 116–124. http://dx.doi.org/10.1016/j.jastp.2011.08.015.

Lary, D., 1997. Catalytic destruction of stratospheric ozone. J. Geophys. Res.: Atmos. 102 (D17), 21515–21526. http://dx.doi.org/10.1029/97JD00912.

Laskar, F.I., McCormack, J.P., Chau, J.L., Pallamraju, D., Hoffmann, P., Singh, R.P., 2019. Interhemispheric meridional circulation during sudden stratospheric warming. J. Geophys. Res. Space Phys. 124 (8), 7112–7122. http://dx.doi.org/10.1029/2018JA026424.

Limpasuvan, V., Orsolini, Y.J., Chandran, A., Garcia, R.R., Smith, A.K., 2016. On the composite response of the MLT to major sudden stratospheric warming events with elevated stratopause. J. Geophys. Res.: Atmos. 121 (9), 4518–4537. http://dx.doi.org/10.1002/2015JD024401.

Limpasuvan, V., Richter, J.H., Orsolini, Y.J., Stordal, F., Kvissel, O.K., 2012. The roles of planetary and gravity waves during a major stratospheric sudden warming as characterized in WACCM. J. Atmos. Sol.-Terr. Phys. 78, 84–98. http://dx.doi.org/10.1016/j.jastp.2011.03.004.

Limpasuvan, V., Thompson, D.W., Hartmann, D.L., 2004. The life cycle of the northern hemisphere sudden stratospheric warmings. J. Clim. 17 (13), 2584–2596. http://dx.doi.org/10.1175/1520-0442(2004)017<2584:TLCOTN>2.0.CO;2.

Liu, H.L., Bardeen, C.G., Foster, B.T., Lauritzen, P., Liu, J., Lu, G., Marsh, D.R., Maute, A., McInerney, J.M., Pedatella, N.M., et al., 2018. Development and validation of the Whole Atmosphere Community Climate Model with thermosphere and ionosphere extension (WACCM-x 2.0). J. Adv. Modelling Earth Syst. 10 (2), 381–402. http://dx.doi.org/10.1002/2017MS001232.

Liu, H.L., Roble, R., 2002. A study of a self-generated stratospheric sudden warming and its mesospheric–lower thermospheric impacts using the coupled TIME-GCM/CCM3. J. Geophys. Res.: Atmos. 107 (D23), ACL–15. http://dx.doi.org/10.1029/2001JD001533.

Ma, Z., Gong, Y., Zhang, S., Xiao, Q., Xue, J., Huang, C., Huang, K., 2022. Understanding the excitation of quasi-6-day waves in both hemispheres during the September 2019 Antarctic SSW. J. Geophys. Res.: Atmos. 127 (3), http://dx.doi.org/10.1029/2021JD035984, e2021JD035984.

Manney, G.L., Schwartz, M.J., Krüger, K., Santee, M.L., Pawson, S., Lee, J.N., Daffer, W.H., Fuller, R.A., Livesey, N.J., 2009. Aura Microwave Limb Sounder observations of dynamics and transport during the record-breaking 2009 arctic stratospheric major warming. Geophys. Res. Lett. 36 (12), http://dx.doi.org/10.1029/2009GL038586.

Marsh, D.R., Mills, M.J., Kinnison, D.E., Lamarque, J.F., Calvo, N., Polvani, L.M., 2013. Climate change from 1850 to 2005 simulated in CESM1 (WACCM). J. Clim. 26 (19), 7372–7391. http://dx.doi.org/10.1175/JCLI-D-12-00558.1.

Matsuno, T., 1971. A dynamical model of the stratospheric sudden warming. J. Atmos. Sci. 28 (8), 1479–1494. http://dx.doi.org/10.1175/1520-0469(1971)028<1479:ADMOTS>2.0.CO;2.

Medvedeva, I., Semenov, A., Pogoreltsev, A., Tatarnikov, A., 2019. Influence of sudden stratospheric warming on the mesosphere/lower thermosphere from the hydroxyl emission observations and numerical simulations. J. Atmos. Sol.-Terr. Phys. 187, 22–32. http://dx.doi.org/10.1016/j.jastp.2019.02.005.

Mlynczak, M.G., 1997. Energetics of the mesosphere and lower thermosphere and the SABER experiment. Adv. Space Res. 20 (6), 1177–1183. http://dx.doi.org/10.1016/S0273-1177(97)00769-2.

Mlynczak, M.G., Hunt, L.A., Lopez-Puertas, M., Funke, B., Emmert, J., Solomon, S., Yue, J., Russell, J.M., Mertens, C., 2021. Spectroscopy, gas kinetics, and opacity of thermospheric nitric oxide and implications for analysis of SABER infrared emission measurements at 5.3 μm. J. Quant. Spectrosc. Radiat. Transfer 268, 107609. http://dx.doi.org/10.1016/j.jqsrt.2021.107609.

Mlynczak, M.G., Hunt, L.A., Thomas Marshall, B., Martin-Torres, F.J., Mertens, C.J., Russell, III, J.M., Remsberg, E.E., López-Puertas, M., Picard, R., Winick, J., et al., 2010. Observations of infrared radiative cooling in the thermosphere on daily to multiyear timescales from the TIMED/SABER instrument. J. Geophys. Res. Space Phys. 115 (A3).

Mlynczak, M.G., Martin-Torres, F.J., Crowley, G., Kratz, D.P., Funke, B., Lu, G., Lopez-Puertas, M., Russell, III, J.M., Kozyra, J., Mertens, C., et al., 2005. Energy transport in the thermosphere during the solar storms of April 2002. J. Geophys. Res. Space Phys. 110 (A12), http://dx.doi.org/10.1029/2005JA011141.

Mlynczak, M., Martin-Torres, F.J., Russell, J., Beaumont, K., Jacobson, S., Kozyra, J., Lopez-Puertas, M., Funke, B., Mertens, C., Gordley, L., et al., 2003. The natural thermostat of nitric oxide emission at 5.3 μm in the thermosphere observed during the solar storms of April 2002. Geophys. Res. Lett. 30 (21), http://dx.doi.org/10.1029/2003GL017693.

Murphy, R., Lee, E., Hart, A., 1975. Quenching of vibrationally excited nitric oxide by molecular oxygen and nitrogen. J. Chem. Phys. 63 (7), 2919–2925. http://dx.doi.org/10.1063/1.431701.

Nath, D., Chen, W., Zelin, C., Pogoreltsev, A.I., Wei, K., 2016. Dynamics of 2013 Sudden Stratospheric Warming event and its impact on cold weather over Eurasia: Role of planetary wave reflection. Sci. Rep. 6 (1), 1–12. http://dx.doi.org/10.1038/srep24174.

Nayak, C., Yiğit, E., 2019. Variation of small-scale gravity wave activity in the ionosphere during the major sudden stratospheric warming event of 2009. J. Geophys. Res. Space Phys. 124 (1), 470–488. http://dx.doi.org/10.1029/2018JA026048.

Ogawa, T., 1976. Excitation processes of infrared atmospheric emissions. Planet. Space Sci. 24 (8), 749–756. http://dx.doi.org/10.1016/0032-0633(76)90111-2.

Pérot, K., Orsolini, Y.J., 2021. Impact of the major SSWs of February 2018 and January 2019 on the middle atmospheric nitric oxide abundance. J. Atmos. Sol.-Terr. Phys. 218, 105586. http://dx.doi.org/10.1016/j.jastp.2021.105586.

Picone, J., Hedin, A., Drob, D.P., Aikin, A., 2002. NRLMSISE-00 empirical model of the atmosphere: Statistical comparisons and scientific issues. J. Geophys. Res. Space Phys. 107 (A12), SIA–15. http://dx.doi.org/10.1029/2002JA009430.

Randall, C., Harvey, V., Singleton, C., Bernath, P., Boone, C., Kozyra, J., 2006. Enhanced NOx in 2006 linked to strong upper stratospheric Arctic vortex. Geophys. Res. Lett. 33 (18), http://dx.doi.org/10.1029/2006GL027160.

Randall, C., Harvey, V.L., Siskind, D., France, J., Bernath, P., Boone, C., Walker, K., 2009. NOx descent in the Arctic middle atmosphere in early 2009. Geophys. Res. Lett. 36 (18), http://dx.doi.org/10.1029/2009GL039706.

Ranjan, A.K., Sunil Krishna, M., Kumar, A., Sarkhel, S., Bharti, G., Bender, S., Sinnhuber, M., 2023. Aspects related to variability of radiative cooling by NO in lower thermosphere, TEC and o/N2 correlation, and diffusion of NO into mesosphere during the Halloween storms. Adv. Space Res. 71 (1), 29–45. http://dx.doi.org/10.1016/j.asr.2022.07.035.

Ranjan, A.K., Sunil Krishna, M., Kumar, A., Sarkhel, S., Chakrabarty, D., Reeves, G., 2023. No radiative cooling and ionospheric response to the hildcaa events following geomagnetic storms. J. Geophys. Res. Space Phys. 128 (12), http://dx.doi.org/10.1029/2023JA032028, e2023JA032028.

Rao, J., Garfinkel, C.I., White, I.P., Schwartz, C., 2020. The Southern Hemisphere minor sudden stratospheric warming in September 2019 and its predictions in S2S models. J. Geophys. Res.: Atmos. 125 (14), http://dx.doi.org/10.1029/2020JD032723, e2020JD032723.

Rozanov, E., Callis, L., Schlesinger, M., Yang, F., Andronova, N., Zubov, V., 2005. Atmospheric response to NOy source due to energetic electron precipitation. Geophys. Res. Lett. 32 (14), http://dx.doi.org/10.1029/2005GL023041.

Russell, III, J.M., Mlynczak, M.G., Gordley, L.L., Tansock, Jr., J.J., Esplin, R.W., 1999. Overview of the SABER experiment and preliminary calibration results. In: Optical Spectroscopic Techniques and Instrumentation for Atmospheric and Space Research III, vol. 3756, International Society for Optics and Photonics, pp. 277–288. http://dx.doi.org/10.1117/12.366382.

Salmi, S.M., Verronen, P., Thölix, L., Kyrölä, E., Backman, L., Karpechko, A.Y., Seppälä, A., 2011. Mesosphere-to-stratosphere descent of odd nitrogen in February–March 2009 after sudden stratospheric warming. Atmos. Chem. Phys. 11 (10), 4645–4655. http://dx.doi.org/10.5194/acp-11-4645-2011.

Sander, S., Friedl, R., Golden, D., Kurylo, M., Moortgat, G., Wine, P., Ravishankara, A., Kolb, C., Molina, M., Finlayson-Pitts, B., et al., 2006. Chemical Kinetics and Photochemical Data for Use in Atmospheric Studies Evaluation Number 15. Technical Report, https://ntrs.nasa.gov/citations/20090033862.

Sassi, F., McCormack, J.P., Tate, J.L., Kuhl, D.D., Baker, N.L., 2021. Assessing the impact of middle atmosphere observations on day-to-day variability in lower thermospheric winds using WACCM-X. J. Atmos. Sol.-Terr. Phys. 212, 105486. http://dx.doi.org/10.1016/j.jastp.2020.105486.

Scherhag, R., 1960. Stratospheric temperature changes and the associated changes in pressure distribution. J. Atmos. Sci. 17 (6), 575–583. http://dx.doi.org/10.1175/1520-0469(1960)017<0575:STCATA>2.0.CO;2.

Schoeberl, M.R., 1978. Stratospheric warmings: Observations and theory. Rev. Geophys. 16 (4), 521–538. http://dx.doi.org/10.1029/RG016i004p00521.

Schofield, K., 1967. An evaluation of kinetic rate data for reactions of neutrals of atmospheric interest. Planet. Space Sci. 15 (4), 643–664. http://dx.doi.org/10.1016/0032-0633(67)90038-4.

Sharma, R., Dothe, H., Duff, J., 1998. Model of the 5.3 μm radiance from NO during the sunlit terrestrial thermosphere. J. Geophys. Res. Space Phys. 103 (A7), 14753–14768. http://dx.doi.org/10.1029/98JA00896.

Sharma, R., Dothe, H., Von Esse, F., 1996. On the rotational distribution of the 5.3-μm "thermal" emission from nitric oxide in the nighttime terrestrial thermosphere. J. Geophys. Res. Space Phys. 101 (A8), 17129–17135. http://dx.doi.org/10.1029/96JA01250.

Shepherd, M., Beagley, S., Fomichev, V., 2014. Stratospheric warming influence on the mesosphere/lower thermosphere as seen by the extended CMAM. In: Annales Geophysicae, vol. 32, (no. 6), pp. 589–608. http://dx.doi.org/10.5194/angeo-32-589-2014.

Shepherd, M.G., Cho, Y.M., Shepherd, G.G., Ward, W., Drummond, J.R., 2010. Mesospheric temperature and atomic oxygen response during the january 2009 major stratospheric warming. J. Geophys. Res. Space Phys. 115 (A7), http://dx.doi.org/10.1029/2009JA015172.

Siskind, D., Coy, L., Espy, P., 2005. Observations of stratospheric warmings and mesospheric coolings by the TIMED SABER instrument. Geophys. Res. Lett. 32 (9), http://dx.doi.org/10.1029/2005GL022399.

Siskind, D.E., Eckermann, S.D., Coy, L., McCormack, J.P., Randall, C.E., 2007. On recent interannual variability of the Arctic winter mesosphere: Implications for tracer descent. Geophys. Res. Lett. 34 (9), http://dx.doi.org/10.1029/2007GL029293.

Smith, A.K., Garcia, R.R., Marsh, D.R., Richter, J.H., 2011. WACCM simulations of the mean circulation and trace species transport in the winter mesosphere. J. Geophys. Res.: Atmos. 116 (D20), http://dx.doi.org/10.1029/2011JD016083.

Smith, A.K., López-Puertas, M., Funke, B., García-Comas, M., Mlynczak, M.G., Holt, L.A., 2014. Nighttime ozone variability in the high latitude winter mesosphere. J. Geophys. Res.: Atmos. 119 (23), 13–547. http://dx.doi.org/10.1002/2014JD021987.

Smith, A., López-Puertas, M., García-Comas, M., Tukiainen, S., 2009. SABER observations of mesospheric ozone during NH late winter 2002–2009. Geophys. Res. Lett. 36 (23), http://dx.doi.org/10.1029/2009GL040942.

Smith, A.K., Marsh, D.R., 2005. Processes that account for the ozone maximum at the mesopause. J. Geophys. Res.: Atmos. 110 (D23), http://dx.doi.org/10.1029/2005JD006298.

Smith-Johnsen, C., Orsolini, Y., Stordal, F., Limpasuvan, V., Pérot, K., 2018. Nighttime mesospheric ozone enhancements during the 2002 southern hemispheric major stratospheric warming. J. Atmos. Sol.-Terr. Phys. 168, 100–108. http://dx.doi.org/10.1016/j.jastp.2017.12.018.

Solomon, S., Crutzen, P.J., Roble, R.G., 1982. Photochemical coupling between the thermosphere and the lower atmosphere: 1. Odd nitrogen from 50 to 120 km. J. Geophys. Res.: Oceans 87 (C9), 7206–7220. http://dx.doi.org/10.1029/JC087iC09p07206.

Tweedy, O.V., Limpasuvan, V., Orsolini, Y.J., Smith, A.K., Garcia, R.R., Kinnison, D., Randall, C.E., Kvissel, O.K., Stordal, F., Harvey, V.L., et al., 2013. Nighttime secondary ozone layer during major stratospheric sudden warmings in specified-dynamics WACCM. J. Geophys. Res.: Atmos. 118 (15), 8346–8358. http://dx.doi.org/10.1002/jgrd.50651.

Varotsos, C., Cracknell, A., Tzanis, C., 2010. Major atmospheric events monitored by deep underground muon data. Remote Sens. Lett. 1 (3), 169–178. http://dx.doi.org/10.1080/01431161003680961.

Varotsos, C., Efstathiou, M., 2018. The observational and empirical thermospheric CO2 and NO power do not exhibit power-law behavior; an indication of their reliability. J. Atmos. Sol.-Terr. Phys. 168, 1–7. http://dx.doi.org/10.1016/j.jastp.2018.01.006.

Wang, Y., Shulga, V., Milinevsky, G., Patoka, A., Evtushevsky, O., Klekociuk, A., Han, W., Grytsai, A., Shulga, D., Myshenko, V., et al., 2019. Winter 2018 major sudden stratospheric warming impact on midlatitude mesosphere from microwave radiometer measurements. Atmos. Chem. Phys. 19 (15), 10303–10317. http://dx.doi.org/10.5194/acp-19-10303-2019.

Yamazaki, Y., Kosch, M.J., Sutton, E.K., 2015. A model of high-latitude thermospheric density. J. Geophys. Res. Space Phys. 120 (9), 7903–7917. http://dx.doi.org/10.1002/2015JA021371.

Yiğit, E., Knížová, P.K., Georgieva, K., Ward, W., 2016. A review of vertical coupling in the Atmosphere–Ionosphere system: Effects of waves, sudden stratospheric warmings, space weather, and of solar activity. J. Atmos. Sol.-Terr. Phys. 141, 1–12. http://dx.doi.org/10.1016/j.jastp.2016.02.011.